ISTITUTO NAZIONALE DI FISICA NUCLEARE

Sezione di Genova

**INFN/TC-08/02**
**23 June 2008**

# STUDY OF THE RESPONSE OF THE NEMO-KM3 DETECTOR INSTRUMENTED WITH DIRECTION-SENSITIVE OPTICAL MODULE

M. Anghinolfi[1], M. Bersani[1], K. Fratini[1], V. Kulikovsky[2],
M. Osipenko[1], A. Plotnikov[2], E. Shirokov[2], M. Taiuti[1] , S. Zavatarelli[1]
on behalf of the NEMO Collaboration
[1)] *INFN, Sezione di Genova, Dip. di Fisica, Univ. di Genova, I-16146 Genova, Italy*
[2)] *Institute of Nuclear Physics, Moscow State University, 119899 Moscow, Russia*

**Abstract**

We studied the performances of the underwater neutrino telescope NEMO-KM3 equipped with direction-sensitive optical modules. The main feature of these optical modules is to detect the direction of the incoming Cherenkov light. In this note we show that the effective area of the underwater neutrino telescope NEMO-KM3 could be improved at low neutrino energies ($E_\nu < 10$ TeV) by adding in the reconstruction procedure the information on the direction of the detected Cherenkov light. As a consequence we show that it is possibile to reduce the number of towers from 81 to 64 maintaining the same effective area of NEMO-KM3.

PACS: 95.55.Vj

*Published by* **SIS-Pubblicazioni**
*Laboratori Nazionali di Frascati*

## 1 Introduction

We investigated how the response of the underwater neutrino telescope NEMO-KM3 [1] could be improved by introducing the additional information of the direction of the detected Cherenkov light. We designed a prototype of a direction-sensitive optical module (**DOM**) and we accordingly modified the simulation and reconstruction codes [2] currently used by the NEMO Collaboration to study the response of the detector. The **DOM** is based on a position-sensitive photomultiplier coupled to a light guide system such that all the Cherenkov light arriving from the same direction is focussed on a reduced area of the photocathode. The basic working principles have been discussed in [3]. In Figure 1 it is summarized how the device would work: all photons arriving from the same direction are collected on a single sector of the multi-anodic photomultiplier.

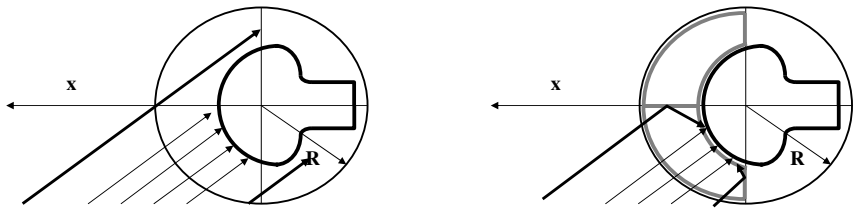


Figure 1: Left: behaviour of the classical optical module: the Cherenkov light illuminates the whole photocathode surface. Right: the mirrors concentrates the light on a single sector of the photocathode surface.

The realization of a prototype of the direction-sensitive optical is in progress. The proposed solution can be integrated in the present design of the NEMO-KM3 detector [4] with minor changes of the telescope geometry. A cross section of the **DOM** prototype is shown in Figure 2. The prototype is based on a 4-anods 10" photomultiplier position-sensitive. In order to match the refraction index of the photomultiplier and the glass sphere, the volume between the photomultiplier and the glass sphere must be filled with a transparent material like plexiglas or optical gel. A set of mirrors realized with highly reflective 3M plastic material with a reflectivity in the blue region better than silver or aluminum concentrate the light on a single sector of the photocathode surface. Two prototypes of such a photomultiplier have been manufactured by Hamamatsu and the measurement of their optical properties is in progress. We will not discuss in this paper the structure of the **DOM**, but we simply assume that the solid angle (close to $2\pi$) cov-

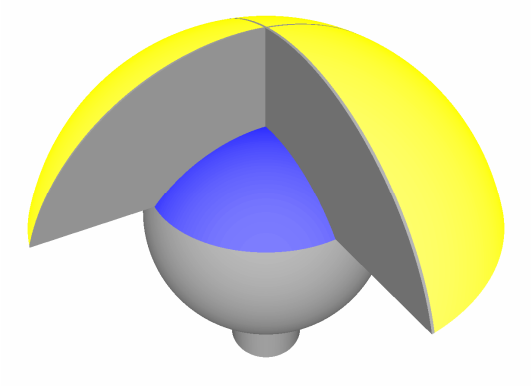

Figure 2: The prototype of a direction-sensitive optical module based on a 4-anodic photomultiplier coupled to a light-guide system. The main components are the photocathode surface (blue), the mirror system (gray) and the optical gel (yellow).

ered by each standard optical module can be subdivided into four independent quadrants. Therefore the new optical module has been implemented in the simulation code using four smaller photomultiplier with reduced angular acceptance. The size of the photocathode area and the cut in the angular acceptance have been defined in order to maintain the same amount of collected light.

The way how the **DOM** has been implemented in the simulation software is discussed in section 2; in section 3 we discuss how we modified the reconstruction program and we show that the response of the telescope based on this solution drastically improves for low energy muons ($E_\mu < 10$ TeV). In section 4 we discuss how the improved performance can be used to design a smaller neutrino telescope with the same detection area of NEMO-KM3.

## 2 The Response of the Direction-Sensitive Optical Module

In this section we briefly verify that the description of the **DOM** is correctly implemented in the simulation program. The standard optical module and the **DOM** configuration have the same sensitive area, therefore the collected light should also be the same. We report in Figure 3 the comparison between the simulations of the amount of light collected with the assumption of zero background (top panel), and with the assumption of 40 kHz background (bottom panel; in Figure 4 the comparison between the number of active optical modules with the assumpion of zero background (top panel), and the same with the assumption of 40 kHz background (bottom panel). The four plots show that there are

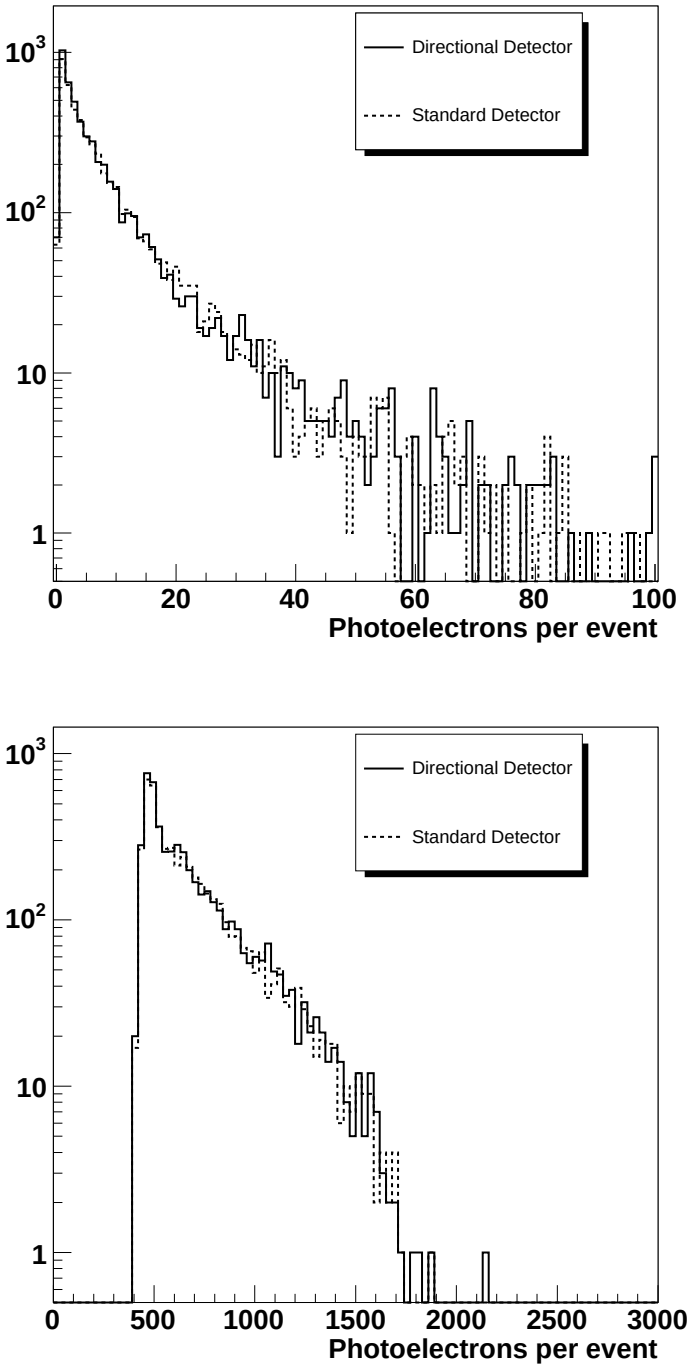


Figure 3: The comparison between the distributions of the light collected in a single event by a detector equipped with standard optical module (dotted histogram) and with **DOM** (continuous histogram) both with the sensitive area of a 10” photomultiplier with zero background (top panel) and with 40 kHz background (bottom panel).

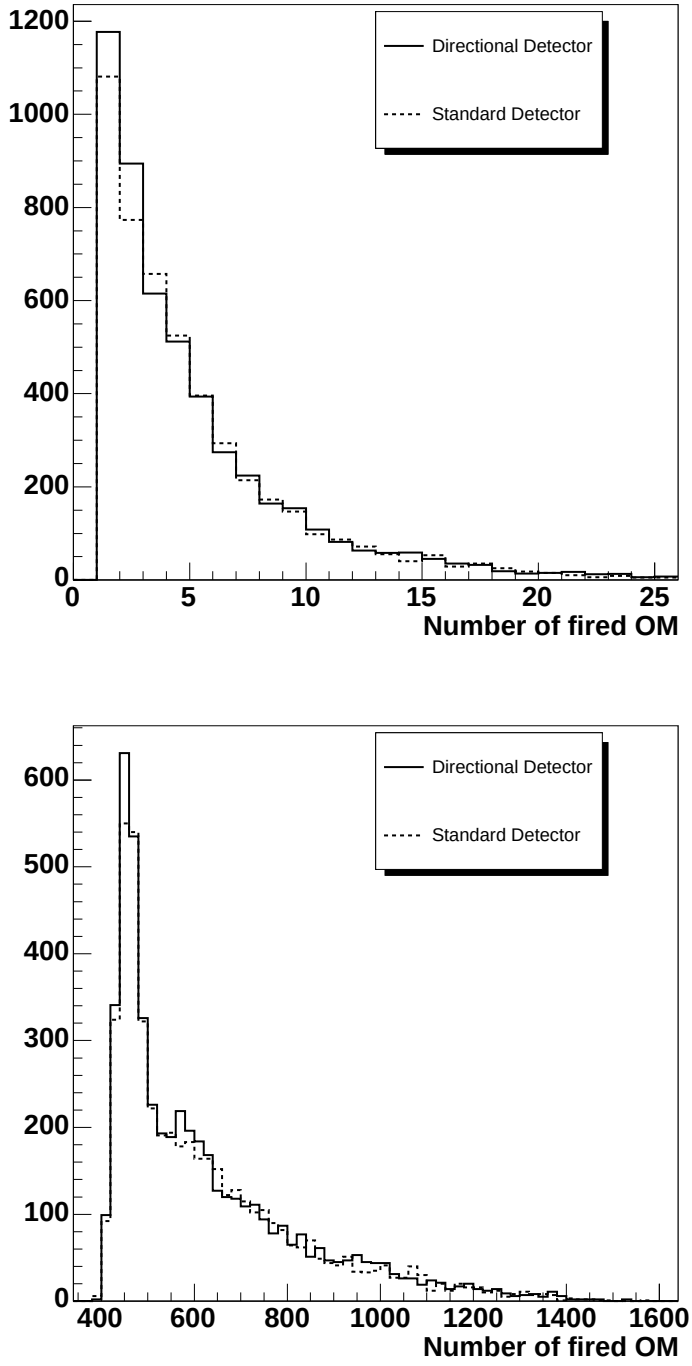


Figure 4: The comparison between the number of active optical modules in the standard configuration and in the **DOM** one with zero background (top panel) and with 40 kHz background (bottom panel).

no differences between the two configurations.

## 3 The Telescope Response

In order to better understand the results, we first remind that the reconstruction program is mainly based on the time response of the photomultipliers. For a given timing value, each active photomultiplier defines in the space an hemi-spherical surface with a thickness proportional to the photomultiplier time resolution as shown in the left panel of Figure 5, representing all the possibile emission points of the detected light.

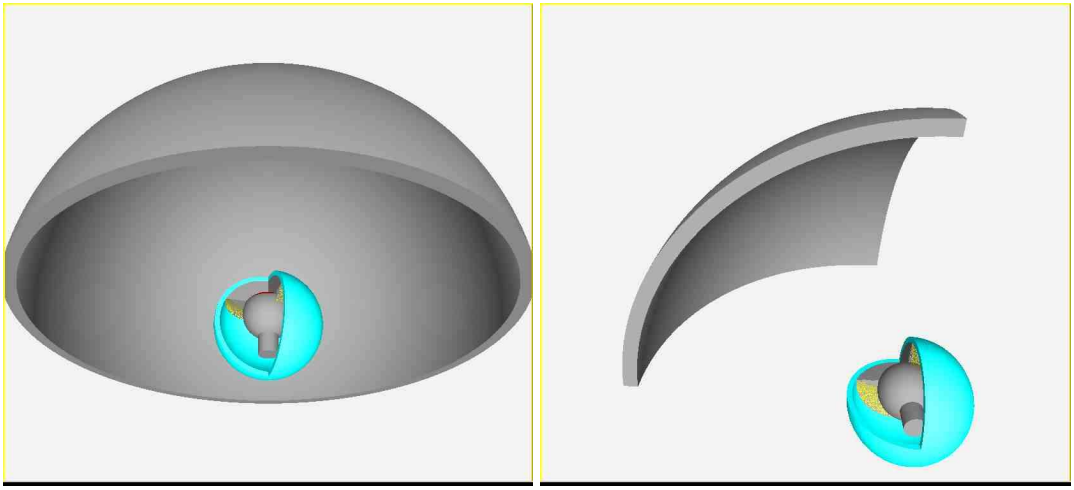

Figure 5: The graphical description of the location of the possible emission point of the Cherenkov light detected by an optical module at fixed timing. The thickness of the gray region corresponds to the photomultiplier time resolution. Left: standard optical module; right: **DOM**.

At least one point of the muon trajectory belongs to the surface and the reconstruction uncertainties clearly increase with the radius of the hemi-spherical surface. For high energy neutrinos ($E_\nu > 10$ TeV) the number of active module is large enough to minimize the uncertainties; but for lower energy neutrino the number of active optical modules decreases and this compensation cannot always occur.

The use of the **DOM** configuration reduces this uncertainty and we anticipate that the effect is particularly evident at neutrino energies smaller than 10 TeV as shown in Figure 9. In fact the surface representing all the possibile emission points of the detected light has now a triangular shape as shown in the right panel of Figure 5. As a consequence, the error on the emission point location is drastically reduced.

The presently available reconstruction software is based on the AART Strategy [5] developed by Aart Heijboer for the ANTARES detector and adapted for the NEMO-KM3. We included the description of the **DOM** modifying few steps of the recostruction code. To better explain the modification we first summarize the AART Strategy.

### 3.1 The AART Strategy

The strategy identifies a reasonable track $T_I$ to be used as the seed for the fit of the data. $T_I$ is estimated by a procedure that includes the following steps: a) the linear fit, b) the M-estimator and c) the fit of the time residuals without noise contribution. As $T_I$ is determined, it is used as input to the final PDF (Probability Density Function) fit that includes the effect of the background.

The AART strategy utilizes for each i-th optical module the local coordinates in the detector, the orientation, the time signal $t_i$ and the collected charge $h_i$. To better describe the invidual steps of the strategy we now define $h_0$ the largest hit that provides the reference time $t_0$ and $c_i$ the flag that identifies the i-th hit that is in coincidence within 20 ns with any other hit in nearby photomultiplier. With this definition we allow, in the case of **DOM**, coincidences in the same optical module.

### 3.2 The Linear Fit

The first step aims to identify a reduced set $\Re_0$ of informations that includes $h_0$ and all hits $h_i$ that have a time difference $\Delta t_i = t_0 - t_i$ such that the following three constraints are simultaneously satisfied

$$\begin{cases} \frac{distance(h_i,h_0)}{c} - 500 \sum\ ns < \Delta t_i \\ \\ \frac{distance(h_i,h_0)}{v} - 20\ ns < \Delta t_i \\ \\ distance(h_i, h_0) < 10\ km \end{cases} \tag{1}$$

where $c$ is the muon velocity and $v$ the speed of light in water. This is a reasonally small set of hits that includes most of the signal hits. However the number of noise hits included in $\Re_0$ is too large and therefore a subset $\Re_L$ is derived from $\Re_0$ choosing all hits with

$$h_i > 2.5\ photoelectrons \quad .OR. \quad c_i = .TRUE. \tag{2}$$

The obtained reduced set $\Re_L$ is the input for the linear fit based on the closest approach distance of the muon track compatible with the hits. Assuming the following muon track equation

$$\vec{y}(t) = \vec{p} + \vec{d} \cdot ct \tag{3}$$

the parameters $\vec{p}$ and $\vec{d}$ that define the track are evaluated minimizing the following sum

$$\sum_{i \in \Re_L} \left[ \vec{C}_i - \vec{y}(t_i) \right]^2 \tag{4}$$

where the closest approach point $\vec{C}_i$ is evaluated from $h_i$ using a table, defined *a priori*, that connects $\vec{C}_i$ to the hit amplitude, and $t_i$ is the measured time. The output of the linear fit is the track $T_L$ that is then utilized as the starting track of the second step of the reconstruction algorithm.

### 3.3 The M-estimator

In order to find the best track, the arrival times of the Cherenkov light $t_i^{th}(T)$, evaluated from a generic track T, are compared to the measured time $t_i$ and the differences (time residuals) $r_i(T) = t_i^{th}(T) - t_i$ minimized. In order to find a solution $T_M$ almost independent from the starting track $T_L$ the M-estimator fit is applied. It minimizes the following function of the residuals $r_i$ and of the photomultiplier angular acceptance

$$G = \sum_{i \in \Re_M} \left[ \kappa \left( -2\sqrt{1 + h_i r_i^2/2} \right) - (1 - \kappa) f_{ang}(cos\theta_i) \right] \tag{5}$$

where $\kappa = 0.05$, $\theta_i$ is the angle of arrival of the light with respect to the axis of the photumultiplier, and the angular acceptance $f_{ang}(cos\theta_i)$ is reported in Figure 6.

The set $\Re_M$ of hits used with the M-estimator fit is the reduced set of $\Re_0$ that satisfies the following constraints

$$\begin{cases} -150\ ns < r_i(T_L) < 150\ ns \\ \\ distance(h_i, T_L) < 100\ m \end{cases} \quad .OR. \quad h_i > 2.3\ photoelectrons \tag{6}$$

### 3.4 The Time Residuals Fit

The track $T_M$ obtained from the M-estimator fit is the seed of the likelihood minimization of the Probability Density Function (PDF) $P(t_i|t_i^{th})$ of the residuals $r_i$, shown in Figure 7

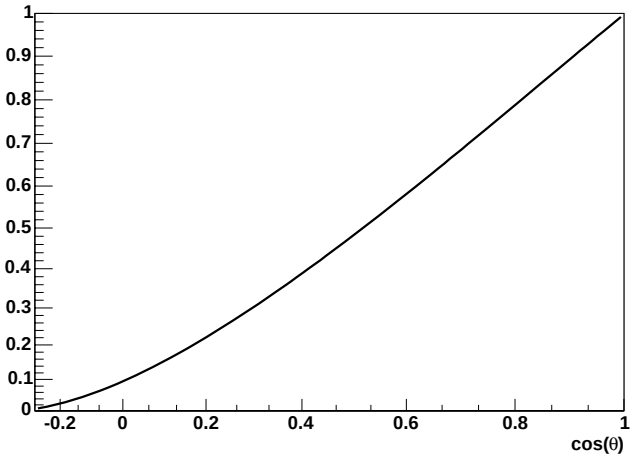


Figure 6: The standard photomultiplier angular acceptance used in the reconstruction.

with the assumption of no background. The set $\Re_{\rm PDF}$ of hits used with the PDF-fit is the reduced set of $\Re_M$ that satisfies the following constraints

$$\begin{cases} -0.5\sigma_r < r_i(T_M) < \sigma_r \\ \\ distance(h_i, T_M) < 300\ m \end{cases}$$
$$.OR.$$
$$h_i > 2.5\ photoelectrons \qquad (7)$$
$$.OR.$$
$$c_i = \ .TRUE.$$

where $\sigma_r$ is the RMS value of the distribution of the residuals $r_i$ referred to $T_M$. In order to further reduce the dependence from the starting track $T_L$, the M-estimator and PDF procedures are repeated several times using different starting tracks $T'_L$ obtained from rotation or translation of the original $T_L$, producing every time a new $T_{PDF}$ track. The $T_{PDF}$ track that shows the best minimization becomes $T_I$, input track for the final fit.

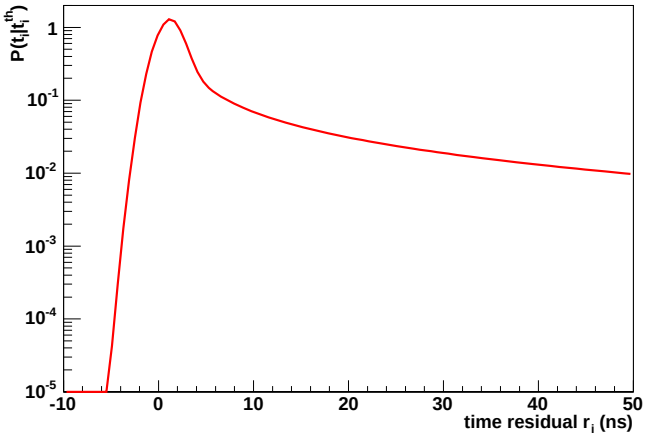


Figure 7: the Probability Density Function (PDF) used in the reconstruction.

### 3.5 The Improved Time Residuals Fit

The final step is based on the likelihood minimization of the improved Probability Density Function (PDF) of the residuals $r_i$ defined as

$$P(t_i|t_i^{th}) = w_{sig}P_{sig}(t_i|t_i^{th}) + (1 - w_{sig})P_{bkg}(t_i|t_i^{th}) \tag{8}$$

where $P_{sig}(t_i|t_i^{th})$ represents the PDF for signal, $P_{bkg}(t_i|t_i^{th})$ represents the PDF for the background noise, and $w_{sig}$, that depends on the amplitude of the read-out, the orientation and location of the optical module, represents the probability that $h_i$ is a signal hit. The used set $\Re_I$ is the subset of $\Re_0$ that satisfies the following constraints:

$$\begin{cases} -250\ ns < r_i(T_I) < 250\ ns \\ \\ distance(h_i, T_I) < 300\ m \end{cases}$$
$$.OR.$$
$$h_i > 2.5\ photoelectrons \tag{9}$$
$$.OR.$$
$$c_i = .TRUE.$$

### 3.6 Implementing the Direction-sensitive Optical Module

The introduction of the direction-sensitive optical module required several changes in the fitting procedure, particularly in the definition of the tables and functions used. First of all the data in the table used in the linear fit have been changed in order to represent the most probable light emission point rather than the closed approach distance. Consequently the linear fit of Eq.(4) has been corrected in order to minimize the light emission point as follows:

$$\sum_i \left[\vec{C}_i - \vec{y}(t'_i)\right]^2 \tag{10}$$

where $t'_i$ is obtained from the measured time $t_i$ correcting for the light propagation from the most probable emission point to the optical module.

In the simulation and reconstruction programs, the angular acceptance $f_{ang}(cos\theta_i)$ was set equal to that shown in Figure 6 for $cos(\theta) > 0.71$ and equal to zero for $cos(\theta) < 0.71$; and the value of $\kappa$ has been optimized to 0.01; in the Improved Time Residual Fit the weight $w_{sig}$ has been modified taking into account also the new expected background rate. The value of $w_{sig}$ has been determined from a MonteCarlo simulation as described in the Aart strategy. In addition to the previous modifications we implemented new constraints in order to efficiently use the information of the direction of the detected light and to optimize the response to low energy neutrino. The modifications to the reconstruction program can be summarized as follows:

a) for low energy neutrinos ($E_\nu < 100\ TeV$), the average number of hits is small and as a consequence the probability that the highest hit $h_0$ is generated by the background is not negligible. Therefore, to improve the reconstruction efficiency, $h_0$ is selected as follows: $h_0 = h_M$ if the largest hit $h_M$ is larger that 3.0 photoelectrons, otherwise $h_0$ is the largest hit with a coincidence signal ($c_M$=.TRUE.);

b) after every fitting procedure described in subsections 3.2 to 3.5, the compatibility between the resulting track and the angular acceptance of the hits used in the reconstruction is verified, the hits not compatible are removed from the set $\Re$ and the fitting procedure is repeated.

c) because in the new geometry the linear fit provides a solution closer to the real track, the range of the rotations used to produce new starting tracks are reduced.

### 3.7 The NEMO-KM3 with the Direction-sensitive Optical Module

We now report the results of the study of the performance of the NEMO-KM3 equipped with **DOM**. We first consider the simulation and reconstruction of neutrinos with energy

below $10^4$ GeV because in this energy interval the average number of signal hits is small and the information on the direction of the detected Cherenkov light can improve the reduction of the background contamination.

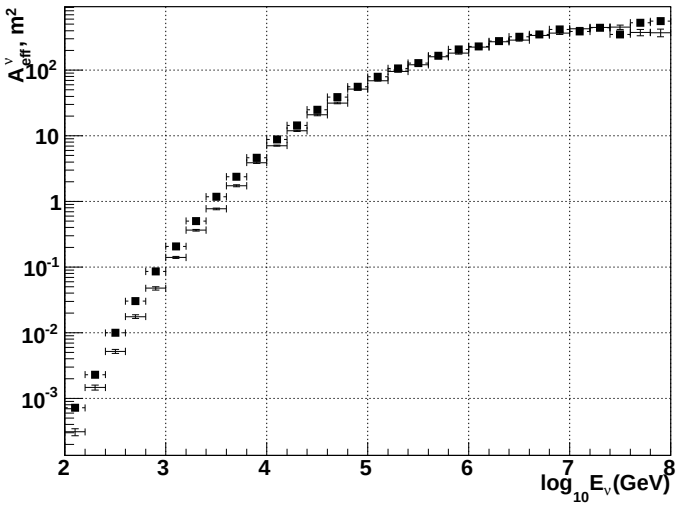


Figure 8: The effective area of the standard NEMO-KM3 detector (crosses) and the NEMO-KM3 detector equipped with **DOM** (black squares) for muonic neutrinos assuming $\Delta\theta < 2^{\circ}$.

To study the detector performances we selected the muonic tracks that have been reconstructed with good angular resolution, that is with an angular difference $\Delta\theta$ between the generated and recostructed muon directions better than $2^{\circ}$. This criteria is clearly not appliable in the real measurement because the value of $\Delta\theta$ is intrinsecally unknown. However, this is the first attempt to introduce the directionality in the reconstruction procedure and we decided to begin with a qualitative estimate of the performances, thus postponing the task of finding the best procedure for low energy muons.

In Figure 8 the comparison between the effective areas of a standard NEMO-KM3 detector and a NEMO-KM3 detector equipped with **DOM** is reported. For sake of completeness we applied to both geometries the check on the compatibility between the resulting track and the angular acceptance of the hitted photomultiplier. The gain is reported in Figure 9 as the ratio between the effective areas of the two studied configurations: the effective area in the **DOM** configuration improves up to a factor 2 at $E_{\nu} = 100$ GeV and the effect is particularly evident at energies $E_{\nu} < 1$ TeV. The knowledge of the direction of the detected Cherenkov light improves the detector capability to reconstruct the muon

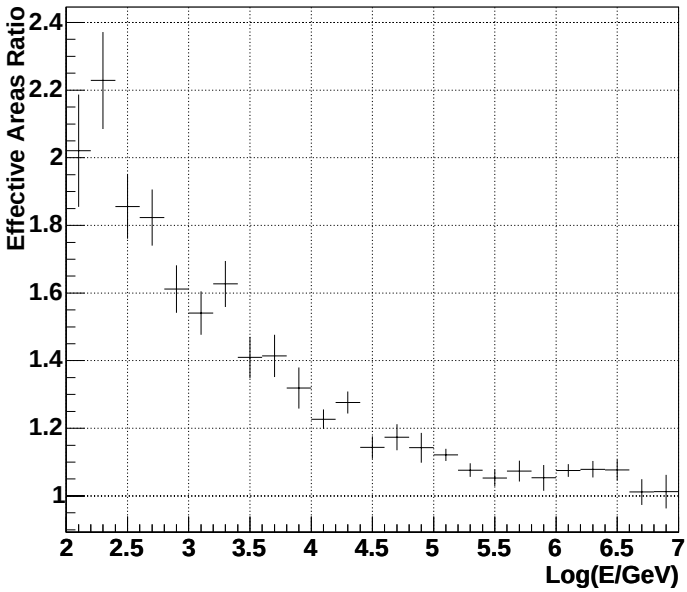


Figure 9: The ratio of the effective areas of the NEMO-KM3 detector equipped with **DOM** and the standard NEMO-KM3 detector.

trajectories. This is shown in Figure 10 where we show, for all reconstructed trajectories, the comparison between the medians of the angular error $\Delta\theta$ distribution for the standard NEMO-KM3 detector and the NEMO-KM3 detector equipped with **DOM**. The **DOM** improves the reconstruction accuracy at neutrino energies below 10 TeV.

We could conclude this section stating that a KM3 detector equipped with **DOM** shows improved performances with respect to a KM3 detector equipped with standard optical modules at neutrino energies below 10 TeV. However in this energy range there is a non negligible contribution from neutrinos originating from the decay of atmosferic muon and by increasing the effective area also the background increases. In addition the extra costs related to the construction of the multianodic photomultiplier and of their light guide system would increase the already high detector value. Therefore we investigate the following alternative solution that could reduce the overall cost of the detector maintaining the already optimized performances.

## 4 A New NEMO-KM3

The NEMO-KM3 geometry is based on a grid 9x9 of 81 towers with interdistance of 140 m and hosts 5184 optical modules. In order to reduce the cost of the detector maintaining

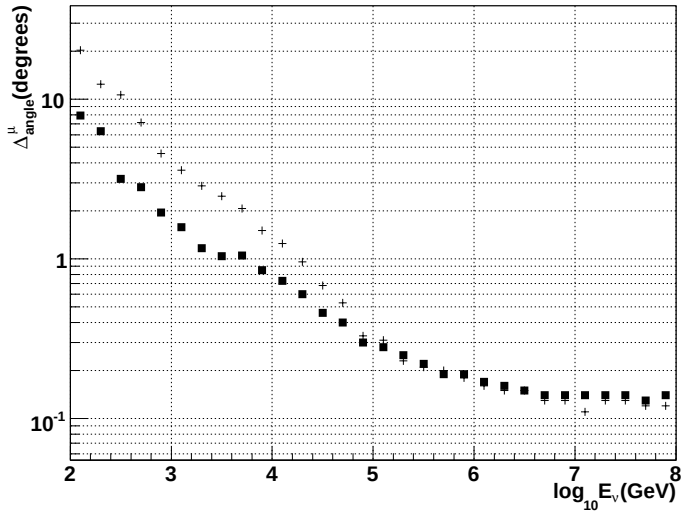


Figure 10: The median of the angular error $\Delta\theta$ of the muon track reconstruction for the standard NEMO-KM3 detector (crosses) and the NEMO-KM3 detector equipped with **DOM** (black squares) for all reconstructed muonic neutrinos.

the same performances we investigated the behaviour of new geometries instrumented with the **DOM**. In particular we studied the effective area of a detector with a reduced number of towers deployed at larger interdistances. A simpler geometry is a reduced grid 8x8 of 64 towers with larger interdistance. We studied two configurations: a) the interdistance equal to 180 m corresponding to an instrumented volume equal to the NEMO-KM3 but with a reduced number of towers (80% of the original quantity); b) the interdistance equal to 200 m corresponding to a larger instrumented volume with, as the previous case, a reduced number of towers (80% of the original quantity). We expect that, due to the increased distance between towers, the reconstruction efficiency for low energy neutrinos should decrease, while for higher energy, where the reconstruction efficiency is related to the instrumented volume, it should remain almost unchanged.

In Figure 11 we report the results of the simulation of a reduced 8x8 NEMO-KM3 with 180 m interdistance instrumented with **DOM** (blue full triangles) and with standard optical modules (magenta empty triangles). For comparison we also included the effective area of the standard NEMO-KM3 geometry (black points). At high neutrino energy the three geometry give the same effective area, while at lower energy the reduced 8x8 NEMO-KM3 instrumented with standard optical module shows worst values. The effect is more evident in Figure 12 where the effective area are reported normalized to the stan-

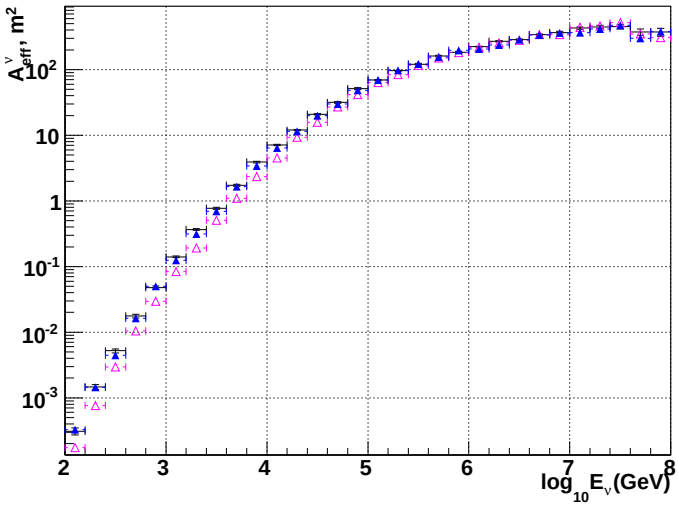


Figure 11: The effective areas of the 8x8 NEMO-KM3 detector with 180 m interdistance equipped with **DOM** (blue full triangles) and equipped with standard optical modules (magenta open triangles). For comparison the effective area of the standard NEMO-KM3 detector is reported (black points).

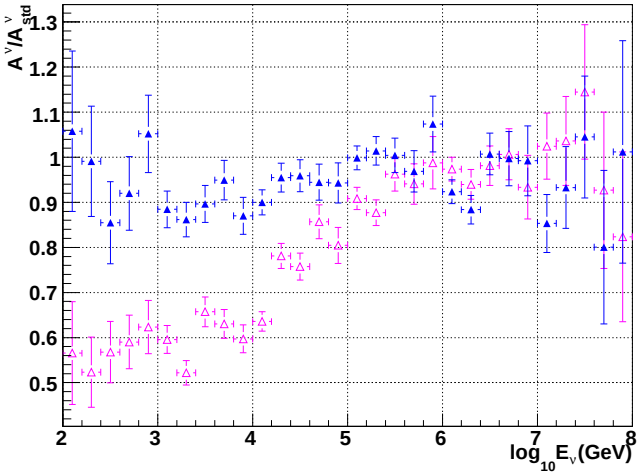


Figure 12: The ratio of the effective areas of the 8x8 NEMO-KM3 detector with 180 m interdistance equipped with **DOM** and the standard 9x9 NEMO-KM3 detector (blue full triangles). For comparison the ratio of the effective areas of the 8x8 NEMO-KM3 detector equipped with standard optical moudules and the standard 9x9 NEMO-KM3 detector (magenta open triangles) is also shown.

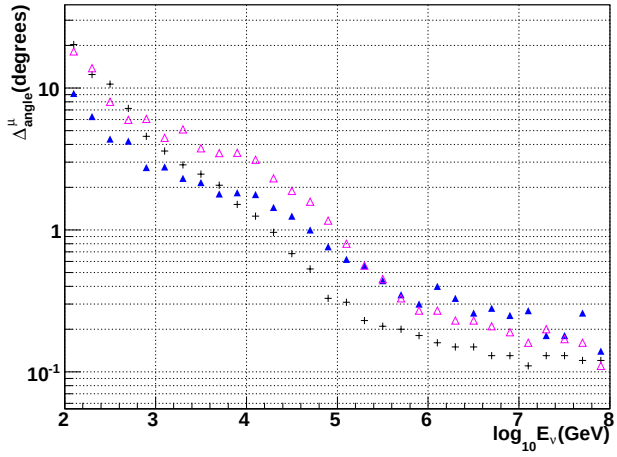


Figure 13: The median of the angular error $\Delta\theta$ of the muon track reconstruction for the 8x8 NEMO-KM3 detector with 180 m interdistance equipped with **DOM** (blue full triangles) and the standard 9x9 NEMO-KM3 detector (black crosses). For comparison $\Delta\theta$ for the 8x8 NEMO-KM3 detector equipped with standard optical modules (magenta open triangles) is also shown.

dard NEMO-KM3 geometry. For the 8x8 NEMO-KM3 instrumented with **DOM** the ratio is, within the statistical errors, larger that 0.9 in the whole energy range. For comparison the effective area of the 8x8 NEMO-KM3 instrumented with standard optical module drops to 0.5 below $E_\nu = 10$ TeV.

The angular resolution is also affected by the geometry. The results are shown in Figure 13 where the median of the $\Delta\theta$ distribution is reported for each simulation. It is clear that the directionality improves the angular resolution at low neutrino energy ($E_\nu = 10$ TeV) while at high energies the sparser geometry degrades the angular resolution but in average it does not exceed twice the value of the standard configuration.

We also studied the effect of increasing the tower interdistance to 200 m in order to increase the instrumented volume. The effective areas normalized to the standard NEMO-KM3 geometry are reported in Figure 14: the new geometry shows at high neutrino energy a larger effective area, but this is obtained at the expenses of a reduction at energies below $E_\nu = 1$ TeV. This effect is more evident in the case of the 8x8 NEMO-KM3 instrumented with standard photomultipliers while for the **DOM** case the ratio is, within the statistical errors, larger that 0.8. The angular resolution, reported in Figure 15 shows a behaviour similar to that previously discussed.

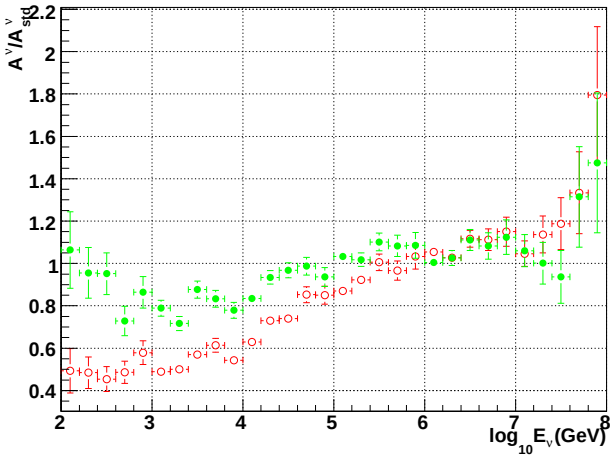


Figure 14: The ratio of the effective areas of the 8x8 NEMO-KM3 detector with 200 m interdistance equipped with **DOM** and the standard 9x9 NEMO-KM3 detector (green full circles). For comparison the ratio of the effective areas of the 8x8 NEMO-KM3 detector with 200 m interdistance equipped with standard optical moudules and the standard 9x9 NEMO-KM3 detector (red empty circles) is also shown.

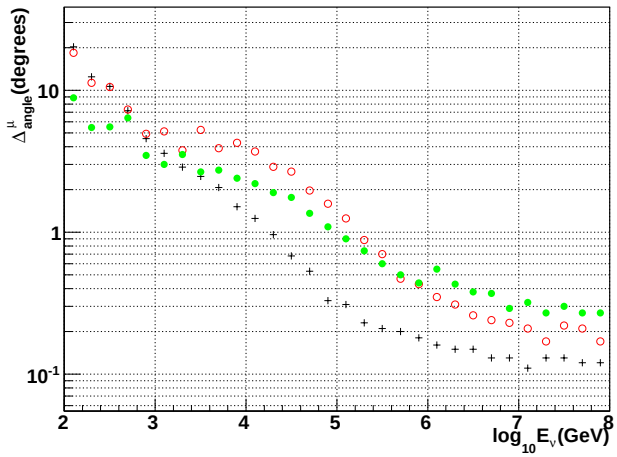


Figure 15: The median of the angular error $\Delta\theta$ of the muon track reconstruction of the 8x8 NEMO-KM3 detector with 200 m interdistance equipped with **DOM** and the standard 9x9 NEMO-KM3 detector (green full circles). For comparison the ratio of the effective areas of the 8x8 NEMO-KM3 detector with 200 m interdistance equipped with standard optical moudules and the standard 9x9 NEMO-KM3 detector (red empty circles) is also shown.

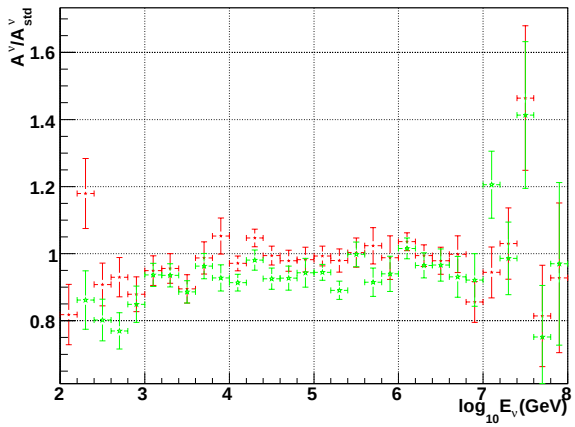


Figure 16: The ratio referred to 1.2 ns TTS sigma of the effective areas of the standard 9x9 NEMO-KM3 detector equipped with **DOM** for different TTS sigma values: 2 ns (red stars), 4 ns (green open stars).

## 5 Conclusions

We implemented in the Antares reconstruction code, starting from the AART strategy, the algorithm to reconstruct the muon trajectory for a neutrino detector equipped with optical module sensitive to the direction of the detected Cherenkov light. With the modified reconstruction code we simulated the NEMO-KM3 geometry instrumented with **DOM** and we compared the performances with those of the standard NEMO-KM3 detector. It resulted that the advantage of using the **DOM** consists in a better reconstruction efficiency of the shortest tracks that originate mainly from low energy neutrinos. Because of the presence of the background that originates from muons decaying in the boreal atmosphere, the improvement of the detector area at low energy would also increase the reconstructed background rate and consequently does not improve the signal-to-background ratio. Therefore we investigated a better use of the **DOM** in a sparser detector that could provide the same detection area of NEMO-KM3 with a reduced number of tower. In particular we proved that a new NEMO-KM3 based on a 8x8 grid of 64 towers with 180 m interdistance and instrumented with the **DOM** would provide the same detection area in the whole neutrino energy range of interest, allowing a potential riduction of the detector cost to approximately 80% the original cost.

## 6 Addendum

¿From the preliminary tests in Catania on the two prototypes of the multi-anodic photomultiplier it resulted that the sigma of the Transit Time Spread is 2 ns, larger than that of the standard 10” photomultiplier. Therefore to study how the new TTS value would affect the detector performancies we simulated the 9x9 geometry with the new timing resolution value and compared the result with the one previously obtained. The results are shown in Figures 16 and **??**. There are no appreciable differences, while for larger TTS sigma values the angular resolution sligthly deteriorates at higher neutrino energies.

## 7 Acknowledgement

We would like to thank the NEMO Collaboration and in particular dr. R.Coniglione and dr. P.Sapienza of the LNS-INFN, for the fruitful discussions and suggestions.

## References

[1] E. Migneco *et al.*, Nucl. Instrum. Meth. A **567** (2006) 444.

[2] `www.antares2.in2p3.fr` ANTARES-soft Internal notes.

[3] M. Taiuti, Nucl. Instrum. Meth. A **525** (2004) 137.

[4] P. Sapienza et al., Proceedings of the First VLVnT Workshop, Amsterdam (2003) in `www.vlvnt.nl/proceedings`.

[5] “An algorithm for track reconstruction in ANTARES” Aart Heijboer ANTARES-soft/20002-002.